ACS OMEGA

Open Access

http://pubs.acs.org/journal/acsodf

Article

Research on Residual Gas Adsorption on Surface of Hexagonal Boron Nitride-Based Memristor

Cheng Ding, Yue Chen, Jin Yang,* Shibin Lu, and Yuehua Dai*

Cite This: *ACS Omega* 2024, 9, 34597−34607

Read Online

ACCESS | Metrics & More | Article Recommendations

ABSTRACT: As a promising nonvolatile memory device with two ends, the memristor has received extensive attention for its industrial manufacture. Density functional theory was used to analyze the adsorption properties of residual gas on hexagonal boron nitride (h-BN)-based memristor model surfaces with Stone−Wales-5577 grain boundary defects [h-BN(SW)]. First, by calculating the adsorption energy, geometric parameters, and charge transfer, we identified the most stable adsorption sites for hydrogen atoms (H-TB1) and H_2 molecules (H_2-TN2). We observed a tendency toward chemisorption for hydrogen atoms and physical adsorption for H_2 molecules at these sites. Furthermore, two coadsorption configurations were formed by introducing H_2 molecules and hydrogen atoms into single adsorption configurations: namely H-TB1_H_2-TN1TN2 and H_2-TN2_H-TB1TN1TN3. In the case of hydrogen-based configuration, there is weak dissociation of the H_2 molecule, which does not facilitate hydrogen atom adsorption. However, adjacent hydrogen atoms tend to form stable dimers, while excess hydrogen atoms have a tendency to weakly chemisorb in the case of H_2-based configuration. The pristine h-BN surface is more favorable for hydrogen atom migration compared to the h-BN(SW) surface due to its higher adsorption energy. On the h-BN(SW) surface, hydrogen atoms tend to migrate inward from the center of adjacent heptagonal boron nitride rings while coadsorption has a minimal impact on their vertical migration as well as that of H_2 molecules. This work provides theoretical insights into the H/H_2 trace gas interaction during h-BN wafer-level fabrication for memristor devices.

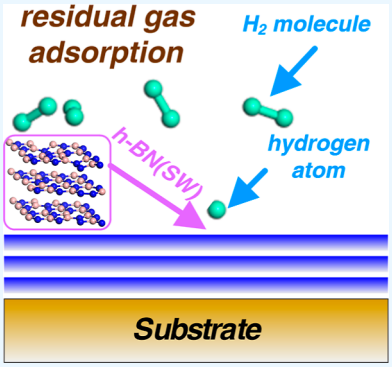

1. INTRODUCTION

With the development of science and technology and the rapid development and innovative application of artificial intelligence, big data and other technologies have posed new technical requirements for nonvolatile data storage.[1−3] The memristor, all two-terminal nonvolatile memory devices based on resistance switching, has been regarded as a competitive candidate for future memory because of its fast reading and writing speeds, low power consumption, and high storage density.[4−6] Hexagonal boron nitride (h-BN), as one of the emerging two-dimensional materials with graphene-like layered structures, can be synthesized by various techniques, such as mechanical stripping, solvent stripping, and chemical vapor deposition (CVD).[7,8] Its application in the memristor field has attracted extensive attention and made a series of progresses in virtue of its unique electrical, mechanical, chemical, and thermal stability properties.[9−13] On the basis of the basic resistance mechanism, that is, the abundant boron vacancy in the h-BN grain boundary promotes the penetration of metal ions between adjacent electrodes to form conductive filaments, a series of strategies for improving the relevant resistance properties and the improvement of experimental preparation technology have been reported. For instance, Au/Ag/h-BN/Fe-based memristor devices have been used to extend iron foil as the substrate material for h-BN film growth, which showed nonvolatile bipolar resistance and volatile threshold traits, respectively, under a negative bias and positive bias voltage.[14] The CVD growth of h-BN on metal foils in the laboratory and transfer to wafers using polymer scaffolds is relatively slow and expensive processes that can result in extensive contamination and cracking. To solve this problem, Lanza's group applied a 30 μm protective layer onto the surface of Ni. As a result, multiple layers of h-BN can be directly grown on Ni-coated Si wafers, and Au/Ti/h-BN/Ni memristor devices can be prepared by the direct evaporation method.[15] Multilayer h-BN thin-film memristor devices have been synthesized by the oxygen-assisted CVD method, and its performance improvement benefitted from the clean and smooth surfaces of O-h-BN thin films and the reduction of grain boundaries.[16] Nevertheless, despite much promise and progress in related research, it remains crucial to achieve controllable wafer-level production for h-BN resistive memory in order to enable large-

Received: March 28, 2024
Revised: July 11, 2024
Accepted: July 15, 2024
Published: July 31, 2024

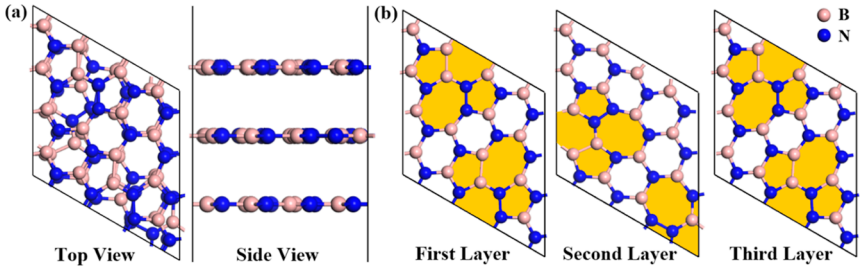

Figure 1. Model of a vertical stack structure with an h-BN(SW) resistance layer is presented. (a) Top and side views are shown. (b) Top view of each layer is illustrated. Pink and blue balls represent B and N atoms, respectively.

scale commercial applications. Encouragingly, Taiwan Semiconductor Manufacturing Corporation has reported a new reliable approach to producing wafer-scale single-crystal h-BN monolayers. This approach involves numerous processes, including the growth of Cu(111) thin films, CVD of h-BN, and transfer of h-BN films onto arbitrary substrates. In this process, vacuum conditions create a clean environment for removing particles, residual gases, and stains. Additionally, trace leakage and residual gas in the vacuum chamber have an important impact on the quality of microelectronic devices. This impact is determined by factors such as the partial pressure of residual gas, metal types used, and maintenance of residual gas analyzer equipment.[17−19] Establishing a reasonable and accurate theoretical calculation model for mechanism analysis and prediction is an important way to address these challenges. First-principles studies can provide atomistic-scale insights into the effect of residual gas on memristor device stability.[20] Previous studies pay more attention on the single adsorption properties of H/H_2 on the surface of monolayer h-BN. For instance, Hao et al. reported a first-principles study on the adsorption of atomic hydrogen on the two-dimensional h-BN monolayer, indicating that the two-dimensional h-BN monolayer is beneficial for high-density hydrogen storage.[21] Petrushenko and Petrushenko conducted density functional theory (DFT) calculations to investigate H_2 adsorption on graphene, h-BN, and other heterostructures, demonstrating that hollow sites are favorable for hydrogen adsorption.[22] To the best of our knowledge, the adsorption of H_2 molecules and hydrogen atoms on three-layer h-BN structures with typical grain boundary defects has not been studied, which is crucial for understanding their effect mechanisms and optimizing design processes.

In this study, by applying DFT, we discerned atomic-level mechanisms for the single adsorption and coadsorption of hydrogen atoms and H_2 molecules on a representative surface of h-BN with a grain boundary defect, i.e., h-BN(SW) surface. Specifically, we focused on the adsorption energy, geometric parameters, electronic structure, charge transfer, and the stable adsorption configuration induced by coadsorption. Moreover, the migration impact of structural and adsorption on the hydrogen atom or H_2 molecules was elucidated with different structural models and migration paths. Our findings provide a new perspective for studying the impact of residual gases, such as H_2 on wafer-level fabrication of h-BN resistive layers.

2. COMPUTATIONAL DETAIL

All calculations in this paper were all based on DFT with the frozen-core projector-augmented wave method as implemented in the Vienna ab initio simulation package.[23,24] The generalized gradient approximation functional of Perdew−Burke−Ernzerhof was used to describe the core and valence electrons in all calculation.[25,26] A cutoff energy of 450 eV was chosen for the plane-wave expansion of the wave functions, while the energy and force convergence criterion for the iterative solution of the Kohn−Sham equations was set to be 10^{-5} eV and 10^{-2} eV/Å. The Grimme's DFT-D3 method was also taken into account van der Waals interactions to improve the theoretical prediction.[27] The migration energy barrier was determined using the climbing image nudged elastic band (CI-NEB) method,[28] with three intermediate images linearly interpolated between initial and final positions. A vacuum region of 20 Å was set to ensure no interaction between surfaces.

To evaluate adsorption stability, adsorption energy (E_{ad}) was calculated by[29,30]

$$E_{ad} = E_{tot} - E_{H/H_2} - E_S$$

where the first and second terms on the right side of the equation correspond to the total energy of the optimized adsorption configuration, and $E_{H/H2}$ represents the energy of H_2 molecule or hydrogen atom optimized, E_S represents the energy of three-layer h-BN(SW) surface optimized, respectively. The ground-state energies of hydrogen atoms and molecules were calculated by using the same method. Negative adsorption energy indicates structural stability through an exothermic reaction. Additionally, a lower adsorption energy corresponds to a more stable structure.

In our previous work, a resistance layer model of multilayer h-BN vertical stack containing a specific distribution of Stone−Wales (SW) grain boundary defects (GBs) has been thoroughly modeled and studied, then the influence mechanism of the coexistence of reactive metal and boron vacancy on the resistance switching performance, interface characteristics between electrode and resistive layers, and graphene intercalation were discussed.[31−33] As shown in Figure 1, the vertical stack model of the h-BN resistance layer within an optimized unit cell (4 × 4 × 1) contained typical topological SW-5577 defects, which were obtained by rotating the B−N bond by 90° to form pairs of pentagons and heptagons (5−7−7−5). During the process, the surface layer was relaxed for optimization, while the lower two layers are fixed for optimization. To benchmark the appropriate exchange correlation functional and calculation parameters, a calculation was performed to investigate the adsorption of a single hydrogen atom on the surface of a pristine h-BN monolayer.

3. RESULTS AND DISCUSSION

3.1. Single Adsorption of Hydrogen Atom and H_2 Molecule. Utilizing this above model, we first studied the single adsorption of hydrogen atom and H_2 molecule on the h-

https://doi.org/10.1021/acsomega.4c02990
ACS Omega 2024, 9, 34597−34607

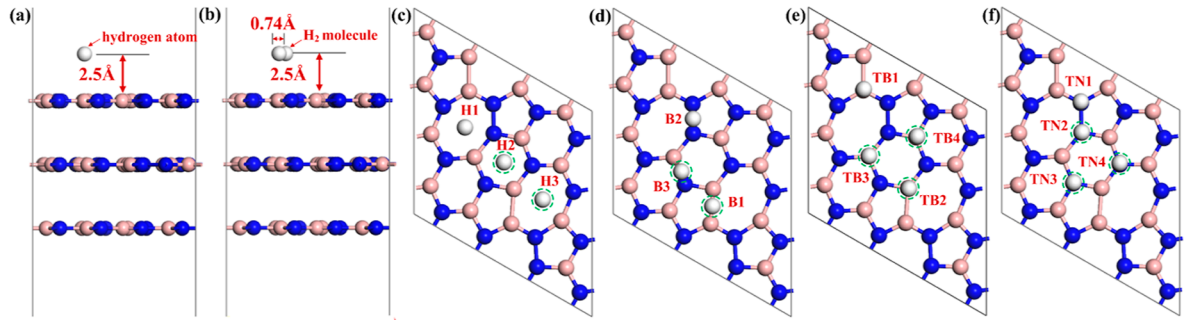

Figure 2. Structure model of the h-BN(SW) model and different adsorption sites of single hydrogen atom and H_2 molecule on the surface before optimization. The side view displays the adsorption models of (a) single hydrogen atom and (b) H_2 molecule. The top view illustrates the adsorption sites for (c) H, (d) B, (e) TB, and (f) TN. Here, H represents the hollow site, B represents the bridge site, and TB/TN represents the top site of boron and nitrogen atoms. Pink balls represent B atoms and blue balls represent N atoms, and while white balls represent H atoms, respectively.

Table 1. Optimized Geometrical and Energy Parameters of Hydrogen Atom and H_2 Molecule Single Adsorption on the h-BN(SW) Surface Were Calculated[a]

	adsorption site	E_{ad} (eV)	d_{H-B} (min) (Å)	d_{H-N} (min) (Å)	$\Delta q\|e\|/\overline{\Delta q\|e\|}$
H	H1	−1.5002	1.258	2.153	0.5664
	H2	−2.2056	1.404	2.207	0.5804
	H3	−1.5025	1.258	2.144	0.5627
	B1	−2.1188	1.346	2.204	0.5785
	B2	−1.4981	1.258	2.143	0.5717
	B3	−1.4606	1.255	2.154	0.5493
	TB1	−2.6956	1.234	2.299	0.5843
	TB2	−2.1178	1.352	2.194	0.5785
	TB3	−1.4983	1.284	2.145	0.5471
	TB4	−1.3134	1.265	2.164	0.5380
	TN1	−2.3847	1.264	2.295	0.5579
	TN2	−1.4761	1.248	2.186	0.5784
	TN3	−2.3123	1.283	2.188	0.5692
	TN4	−2.0527	1.296	2.130	0.5812
H_2	H1	−0.0385	2.820	2.839	0.0615
	H2	−0.0350	2.861	2.863	0.0640
	H3	−0.0197	2.749	2.715	0.0651
	B1	−0.0314	2.801	3.072	0.0441
	B2	−0.0410	2.924	2.682	0.0647
	B3	−0.0369	3.090	2.857	0.0412
	TB1	−0.0565	2.851	2.875	0.0395
	TB2	−0.0347	2.846	2.875	0.0459
	TB3	−0.0573	2.702	2.781	0.0475
	TB4	−0.0240	2.680	2.851	0.0583
	TN1	−0.0736	2.977	3.015	0.0436
	TN2	−0.0899	2.994	2.974	0.0638
	TN3	−0.0089	2.998	2.878	0.0458
	TN4	−0.0055	2.980	2.844	0.0458

[a]The calculated adsorption energies (E_{ad}), displacement of the nearest boron/nitrogen atom from the hydrogen atom (d_{H-B} (min), d_{H-N} (min)), and Bader charge transfer ($\Delta q|e|$) per hydrogen atom at 11 possible adsorption sites were presented.

BN(SW) model surface. As shown in Figure 2, there are three types of typical adsorption sites for the hydrogen atom: the hollow site (H site), where the hydrogen atom sits above the center of a hexagonal ring; the bridge site (B site), where the hydrogen atom coordinates with the boron−nitrogen bond; and the top site, - where the hydrogen atom locates directly above a boron atom (TB site) or a nitrogen atom (TN site). The initial adsorption position of a H_2 molecule aligns with that of a single hydrogen atom. The initial adsorption position of an H_2 molecule aligns with that of a single hydrogen atom.

The h-BN(SW) model structure containing SW-5577 defects was optimized. Subsequently, the individual adatoms were placed at three different types of initial sites, and the overall structure was optimized again to minimize the system's energy. Depending on the initial site of hydrogen atom and H_2 molecule, the adsorption energies (E_{ad}) as well as the displacement of the nearest boron/nitrogen atom of the hydrogen atom [d_{H-B} (min), d_{H-N} (min)] and Bader charge transfer ($\Delta q|e|$) per hydrogen atom are summarized in Table 1.

The TB1 site was found to be the most favorable adsorption site for a single hydrogen atom, with a higher adsorption

https://doi.org/10.1021/acsomega.4c02990
ACS Omega 2024, 9, 34597−34607

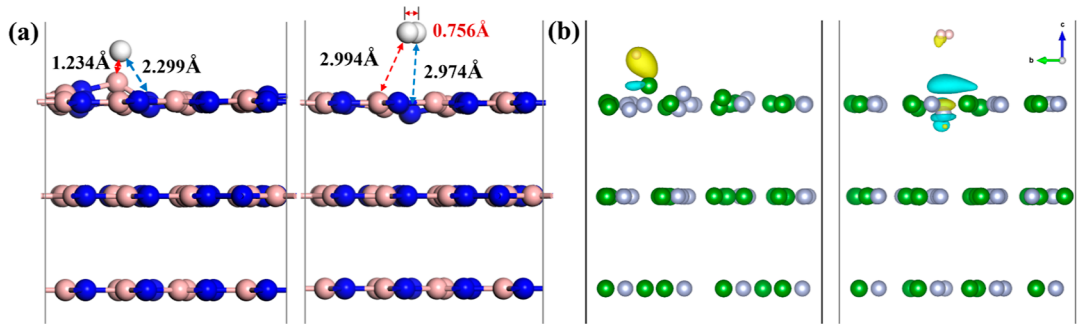

Figure 3. (a) Side views of optimized structures for single adsorption of a hydrogen atom at the TB1 site and an H_2 molecule at the TN2 site (with white-, blue-, and pink-colored atoms representing H, B, and N, respectively). (b) Differential charge density diagram of the adsorption configuration for a single hydrogen atom at the TB1 site and an H_2 molecule at the TN2 site (the electron density isosurface is 0.015 e/Å^3, with yellow indicating an increase in charge density and blue-green indicating a decrease in charge density).

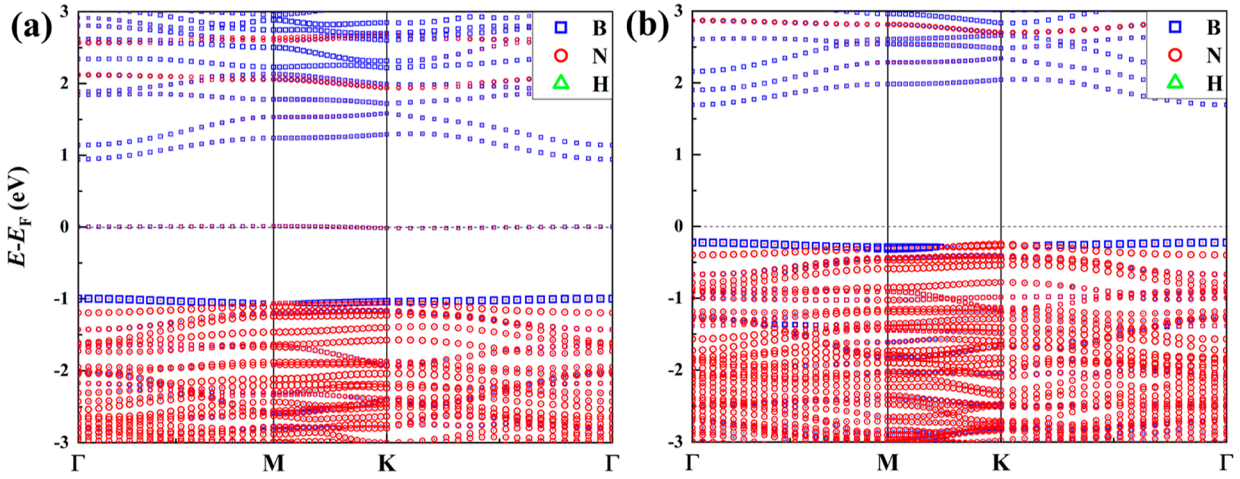

Figure 4. Projected band structure of the adsorption configuration obtained by single adsorption of (a) hydrogen atom at the TB1 site and (b) H_2 molecule at the TN2 site.

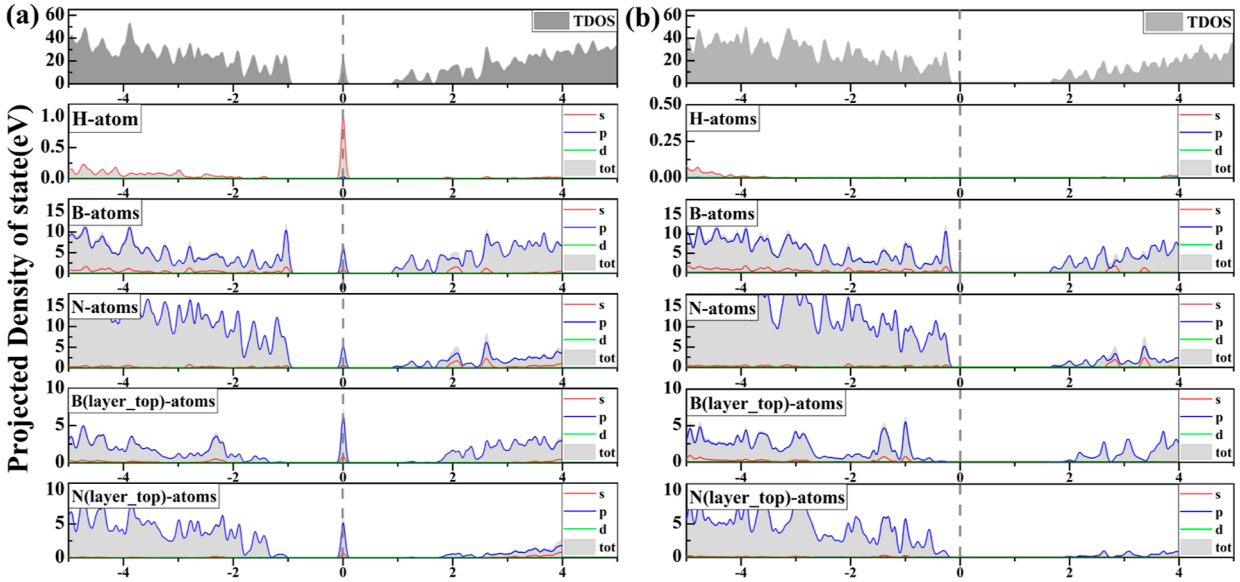

Figure 5. Projected density of states (PDOS) is obtained by single adsorption of (a) hydrogen atom at the TB1 site and (b) H_2 molecule at the TN2 site.

energy (−2.6956 eV) compared with other sites. The absolute values of the adsorption energies ranged from −2.2056 to −1.4606 eV for H and B sites and from −2.3847 to −1.4761 eV for TN sites, respectively. We found that the TB1 site exhibited the closest adsorption geometry, with an interatomic distance of 1.234 Å between the hydrogen atom and its nearest

https://doi.org/10.1021/acsomega.4c02990
ACS Omega 2024, 9, 34597−34607

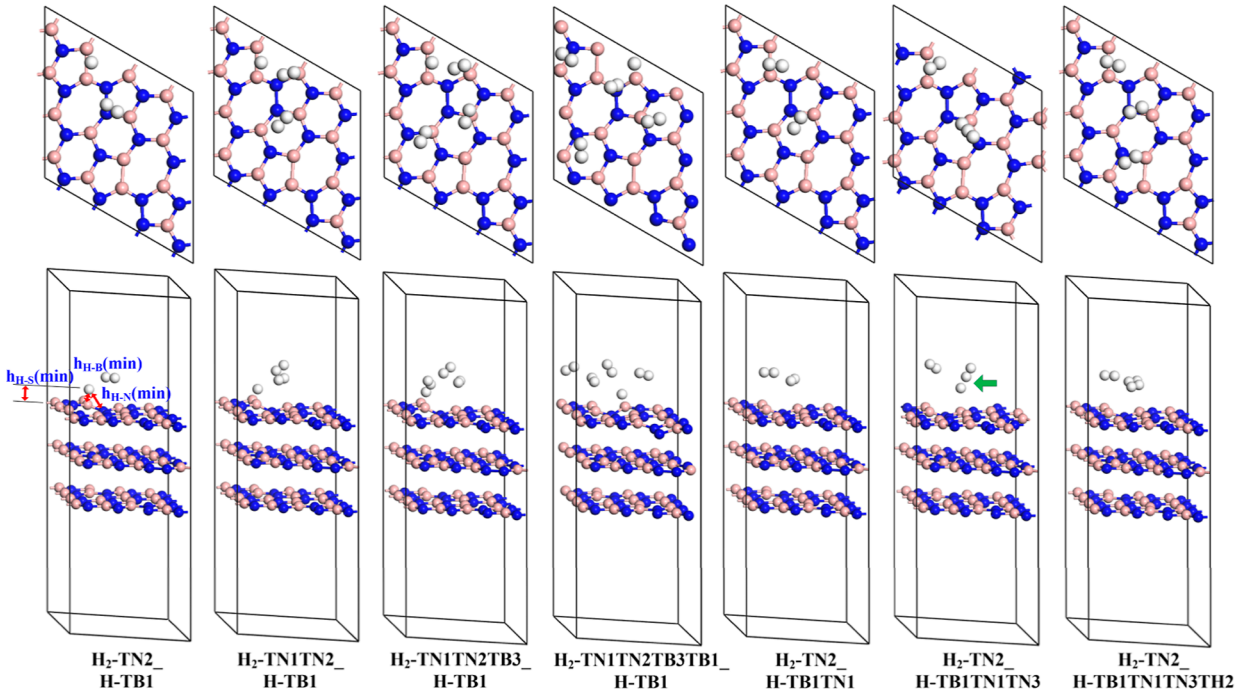

Figure 6. Side views of optimized structures of seven coadsorption models in the H-based case (H_2-TN2_H-TB1, H_2-TN1TN2_H-TB1, H_2-TN1TN2TB3_H-TB1, and H_2-TN1TN2TB3TB1_H-TB1) and in the H_2-based case (H_2-TN2_H-TB1TN1, H_2-TN2_H-TB1TN1TN3, and H_2-TN2_H-TB1TN1TN3TH2) h_{H-B} (min) or h_{H-N} (min) is a minimum bond distance between the adsorbed H atom and its neighboring surface B atom or N atom, and h_{H-S} (min) indicates the minimum adsorption height of hydrogen atoms with respect to the first layer.

neighbor boron atoms as well as a distance of 2.299 Å for nitrogen atoms. Additionally, at the TB1 site, there was a maximum charge transfer (0.5843*e*), leading to an enhanced covalent bond between the hydrogen atom and the h-BN(SW) surface, thereby increasing its adsorption capacity. Furthermore, when considering parameters for H_2 molecule adsorption at each individual site, we found that their respective adsorption energies ranged from approximately −0.0899 to −0.0055 eV, which were significantly lower than those observed for single hydrogen atom adoptions mentioned earlier. Notably, in all optimized configurations corresponding to initial adsorption sites mentioned above, both H−B and H−N bond lengths were notably increased compared to those in single hydrogen atom adoptions; specifically reaching 2.680 and 2.682 Å, respectively. For all H_2 molecule sites considered here, the charge transfer per hydrogen atom varied between 0.0395*e* and 0.0651*e* was significantly reduced when compared with single hydrogen atom adoptions discussed previously. The TN2 site exhibited the lowest absorption energy (−0.0899 eV), with an amount of charge transfer equaling 0.0638*e*. The results indicate that the adsorption energy of H/H_2 has a magnitude equal to that of the pristine monolayer h-BN in previous literature studies, which validates the accuracy of the calculation details.[22,34]

The corresponding values for the adsorption of H_2 molecules at the TN2 site are 2.994 and 2.974 Å, respectively, as shown in Figure 3, compared with the H−B and H−N bond lengths of the most stable adsorption sites of single hydrogen atoms (1.234 and 2.299 Å). Additionally, the distance of two hydrogen atoms increased from 0.74 Å at the initial stage to 0.756 Å after adsorption optimization. A differential charge density diagram for two adsorption configurations were plotted, charge accumulation occurred on the surface of the h-BN(SW) layer near the adsorbed atoms. The charge accumulation of the single hydrogen atom represented by the TB1 site was significantly higher than that of the H_2 molecule represented by the TN2 site, demonstrating a pronounced disparity in their respective charge distributions.

The projected band structure and PDOS are plotted in Figures 4 and 5 to understand the electronic structure and bond characteristics between the adsorbed atom and surface resulting from single adsorption of a hydrogen atom at the TB1 site and an H_2 molecule at the TN2 site. For the single adsorption of a hydrogen atom at the TB1 site, the H 1s states are located below and above the Fermi level, exhibiting a strong interaction with the B 2p and N 2p levels. This strong orbital hybridization results in a decrease in short-range repulsion force and improves the stability of the adsorption system. Combined with charge transfer, this suggests that hydrogen atoms tend to form chemical bonds with h-BN(SW) surface atomic layers. Due to weak van der Waals interactions between layers, the first h-BN(SW) surface layer plays a crucial role in determining the electronic structure. The valence-band maximum (VBM) states within an energy range of −3 to −1 eV are mainly contributed by N 2p orbitals, while conduction band maximum (CBM) states within an energy range of 1−3 eV are mainly contributed by B 2p orbitals. In Figure 5b, when an H_2 molecule is adsorbed on the TN2 site, there is less charge transfer due to the longer distance between the H_2 molecule and two-dimensional h-BN(SW) surface compared to hydrogen atoms. The difference in total density of state (TDOS) near the VBM and CBM is small compared to hydrogen atoms as well. Although there remains about a 2 eV band gap, overall guide bands shift approximately by 1 eV; however, there is no obvious orbital hybridization between hydrogen elements and boron/nitrogen elements in this middle region of the band gap. These results suggest that while hydrogen atoms chemically adsorb at TB1 sites on h-

https://doi.org/10.1021/acsomega.4c02990
ACS Omega 2024, 9, 34597−34607

Table 2. Optimized Geometrical and Energy Parameters of Hydrogen Atom and H_2 Co-Adsorption configurations on the h-BN(SW) Surface[a]

base	configuration	E_{ad} (eV)	d_{H-B} (min) (Å)	d_{H-N} (min) (Å)	h_{H-S} (min) (Å)	$\overline{\Delta q\|e\|}$
H-TB1	H_2-TN2	−1.881	1.439	2.227	1.273	0.118
	H_2-TN1TN2	−2.289	1.347	2.241	1.256	0.137
	H_2-TN1TN2TB3	−1.640	1.356	2.222	1.273	0.107
	H_2-TN1TN2TB3TB1	−0.879	1.199	2.328	1.304	0.086
H_2-TN2	H-TB1	−1.881	1.439	2.227	1.273	0.118
	H-TB1TN1	−1.210	2.882	3.069	2.639	0.042
	H-TB1TN1TN3	−1.430	2.222	2.613	2.199	0.047
	H-TB1TN1TN3TH2	−1.219	2.873	3.017	2.665	0.038

[a] E_{ad} refers to adsorption energy, h_{H-B} (min) or h_{H-N} (min) is minimum bond distance between the adsorbed H atom and neighbor surface B atom or N atom, h_{H-S} (min) indicates the minimum adsorption height of H atoms with respect to the first layer, and $\overline{\Delta q|e|}$ denotes Bader charge transfer per hydrogen atom.

BN(SW) surfaces, H_2 molecules physically adsorb at TN2 sites.

3.2. Co-Adsorption of Hydrogen Atom and H_2 Molecule. Experimentally, it has been suggested that the preparation and growth of h-BN involves annealing and cooling in the hydrogen stream, which may cause dissociation of H_2 molecules into hydrogen atoms at high temperatures.[17−19] Therefore, we considered the coadsorption behavior of both hydrogen atoms and H_2 molecules on the h-BN(SW) surface as discussed above.

According to the initial adsorption positions and quantity occupied by H_2 molecules adjacent to the surface layer in the H-based case, seven coadsorption configuration models were defined and optimized for both the H-based case and the H_2-based case, as shown in Figure 6. Among them, for the H-based case, the most stable single adsorption configuration of a hydrogen atom (H-TB1) was chosen as the basis for coadsorption. For the H_2-based case, the most stable single adsorption configuration of an H_2 molecule (H_2-TN2) was defined as its basis. The optimized geometrical and energy parameters of hydrogen atoms and H_2 coadsorption configurations are summarized in Table 2.

According to Figure 6 and Table 2, in the H-based case, these four stable coadsorption configurations show slight changes in bond length and different distribution states in space for H_2 molecules, but significant dissociation does not occur. The adsorption energy ranges from −2.289 to −0.879 eV, with hydrogen atoms located at the lowest point of the adsorption configuration defining the minimum adsorption height. As the number of H_2 molecules increases, the adsorption energy of coadsorption configurations first increases and then decreases; among them, the H-TB1_H_2-TN1TN2 configuration has the highest adsorption energy (−2.289 eV) and lowest adsorption height (1.256 Å), indicating its stability as compared to others. Furthermore, considering the atomic position and charge transfer after adsorption, the boron−hydrogen atom distance is at least 1.347 Å in all four configurations with an average charge transfer up to 0.137*e* per atom transferred during this process; however, it should be noted that increasing H_2 molecule numbers cannot enhance hydrogen atom's absorption strength. Analyses of the adsorption characteristics showed that, for the H_2-based case, adding 1−4 hydrogen atoms near the initial site of the H_2 molecule single adsorption (H_2-TN2), resulted in a more favorable coadsorption configuration with one or three hydrogen atoms and an H_2 molecule compared to two or four atoms. The average adsorption energies reached −1.881 and −1.430 eV, respectively. In particular, when there were two or more hydrogen atoms in the configuration, the shortest distance between the hydrogen atom with the lowest adsorption height and the boron atom in the coadsorption configuration containing three hydrogen atoms was found to be 2.222 Å, with a corresponding average atomic charge transfer of 0.047*e*. Therefore, it was determined that coadsorption of H_2-TN2_H-TB1TN1TN3 configuration had the most favorable adsorption energy in this case. The geometrical and energy parameters indicated that every two adjacent hydrogen atoms tended to form a stable dimer configuration when an even number of hydrogen atoms were coadsorbed with H_2 molecules on the h-BN(SW) surface. When an odd number of hydrogen atoms were present, any excess single atom would be adsorbed near the top site of a boron atom with a lower adsorption height and distance from it resulting in greater charge transfer from hydrogen atoms to the h-BN(SW) surface.

According to the differential charge diagram in Figure 7 for the coadsorption configuration, the results demonstrate that

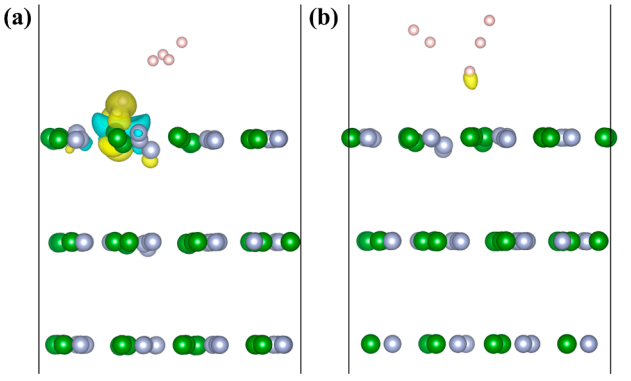

Figure 7. Differential charge density diagram of coadsorption configuration of (a) H-TB1_H_2-TN1TN2 and (b) H_2-TN2_H-TB1TN1TN3 (electron density isosurface is 0.015 e/Å^3, yellow indicates an increase in charge density, while blue−green indicates a decrease in charge density).

the hydrogen atom with the lowest adsorption height gains electrons, and there is a significant increase in charge density in the H-TB1_H_2-TN1TN2 coadsorption configuration. However, compared to the H-base configuration, the H_2-TN2_H-

https://doi.org/10.1021/acsomega.4c02990
ACS Omega 2024, 9, 34597−34607

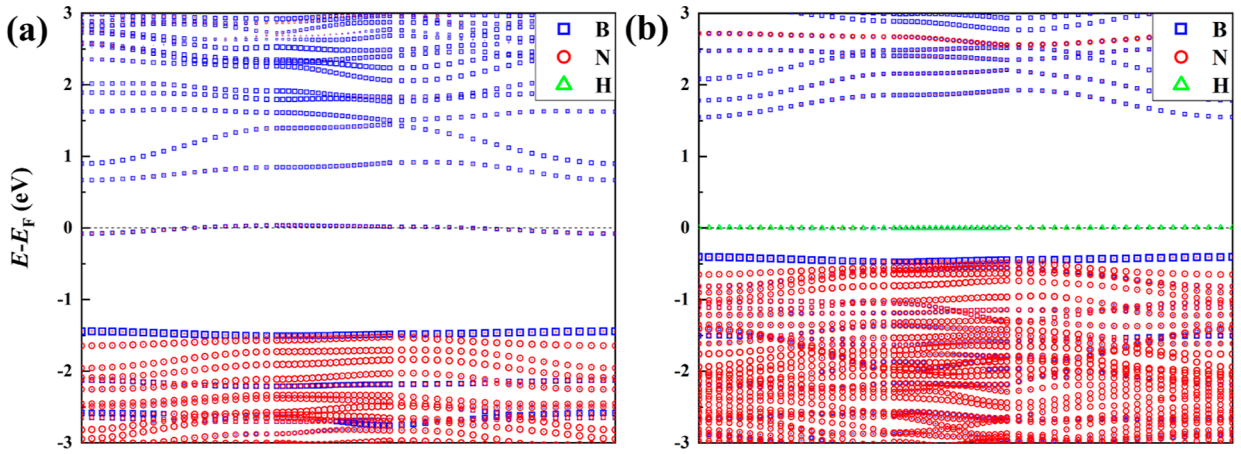

Figure 8. Projected band structure of the coadsorption configuration of (a) H-TB1_H_2-TN1TN2 and (b) H_2-TN2_H-TB1TN1TN3.

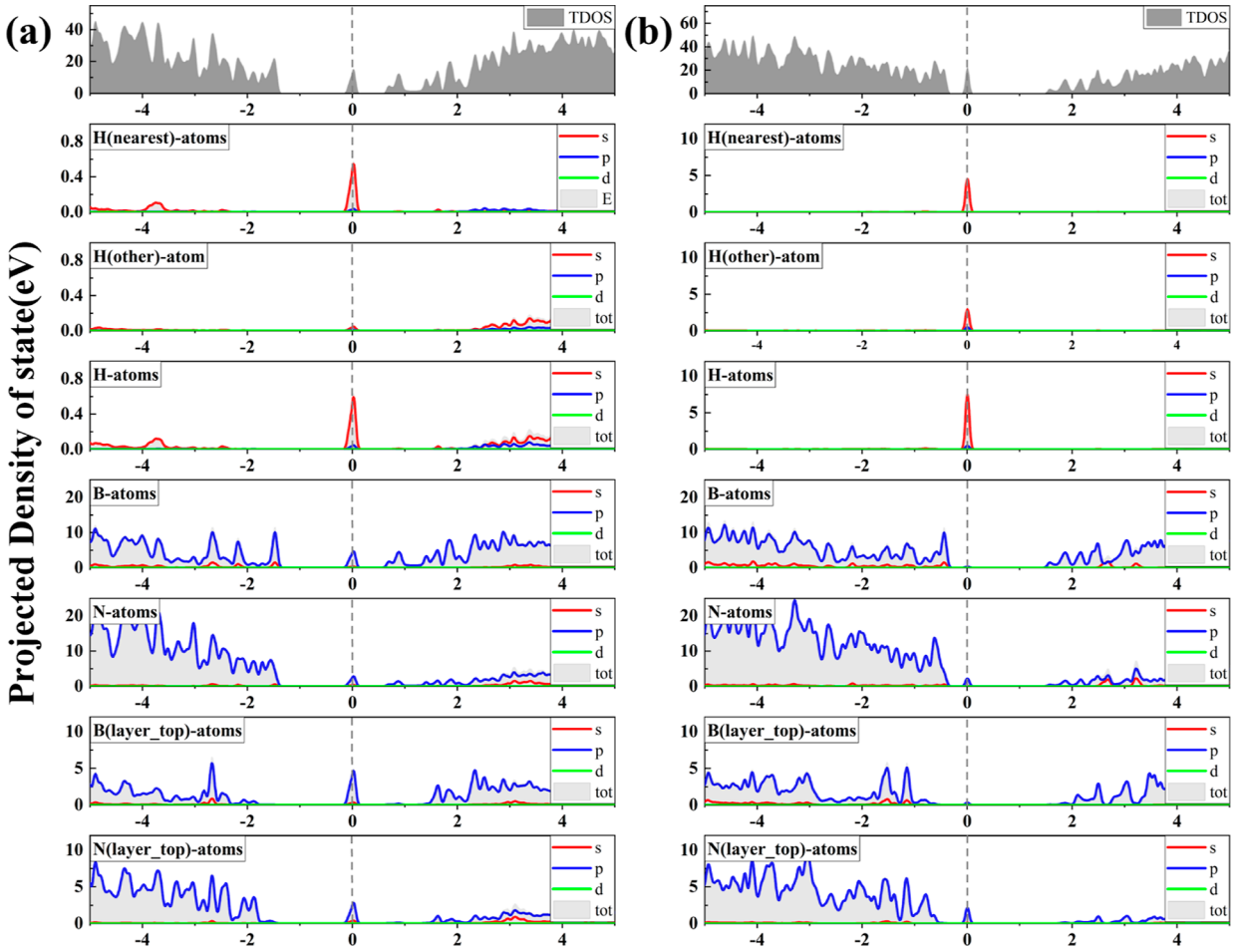

Figure 9. PDOS of the coadsorption configuration of (a) H-TB1_H_2-TN1TN2 and (b) H_2-TN2_H-TB1TN1TN3.

TB1TN1TN3 configuration shows a noticeably weaker charge accumulation intensity.

In Figure 8, the projected band structures of H-TB1_H_2-TN1TN2 and H_2-TN2_H-TB1TN1TN3 configurations were calculated to investigate the electronic properties of the coadsorption system. Compared with the single adsorption of a hydrogen atom at the TB1 site, the bandwidth of the coadsorption configuration of H-TB1_H_2-TN1TN2 remained approximately 2 eV, but the Fermi level became closer to the CBM with the addition of H_2 molecules. For the coadsorption configuration of H_2-TN2_H-TB1TN1TN3 with three single hydrogen atoms entering into the model, both CBM and VBM decreased by about 0.2 eV relative to the Fermi level, and an impurity level contributed by hydrogen atoms appeared near it.

The PDOS analysis of the H-TB1_H_2-TN1TN2 configuration in Figure 9a revealed a shift of the Fermi levels toward higher energies closer to the CBM, accompanied by a clear observation of midgap states. These midgap states were predominantly occupied by H 1s, B 2p, and N 2p electrons due to strong orbital hybridization resulting from chemisorption of

https://doi.org/10.1021/acsomega.4c02990
ACS Omega 2024, 9, 34597−34607

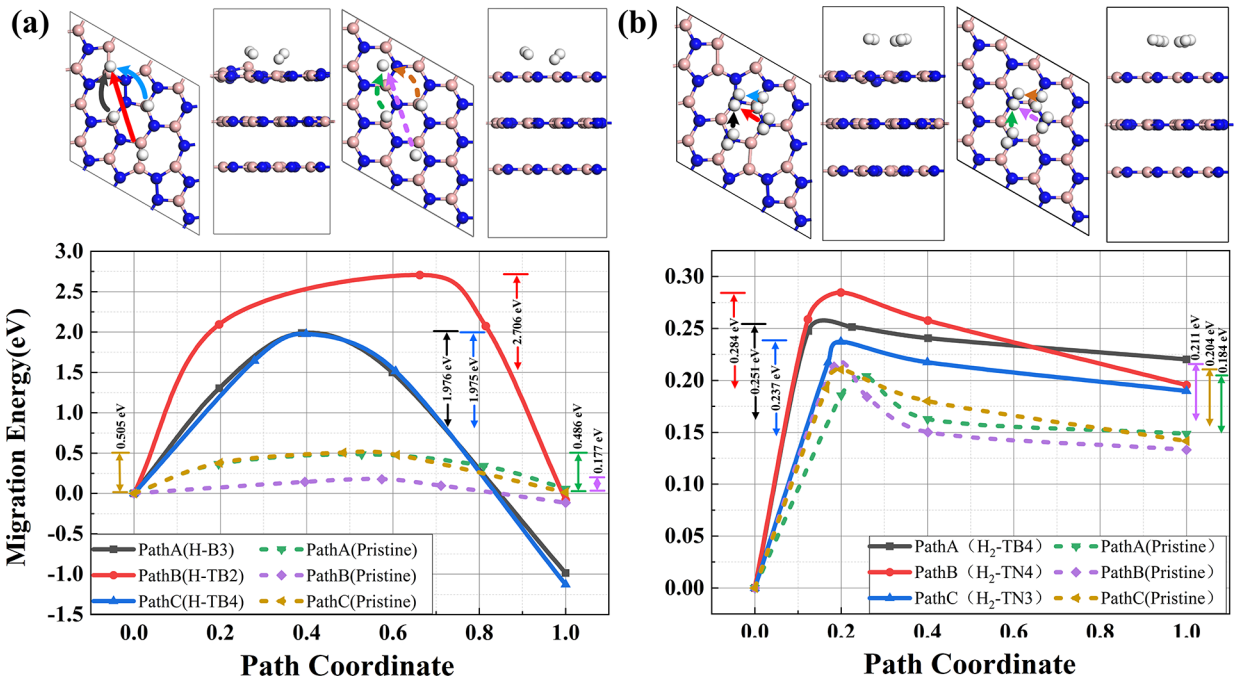

Figure 10. (a) Schematic diagram of three typical migration paths for a hydrogen atom between the initial sites (H-B3, H-TB2, and H-TB4) and the final site (H-TB1) over two h-BN model surfaces, including the h-BN(SW) model and the pristine h-BN model. The calculated migration barrier corresponds to the above migration paths of a hydrogen atom. (b) Schematic diagram of three typical migration paths for a H_2 molecule between the initial sites (H_2-TB4, H_2-TN4, and H_2-TN3) and the final site (H_2-TN2) over two model surfaces, including the h-BN(SW) model and the pristine h-BN model. The calculated migration barrier corresponds to the migration path of a H_2 molecule. The white, blue, and pink balls represent hydrogen atoms, nitrogen atoms, and boron atoms.

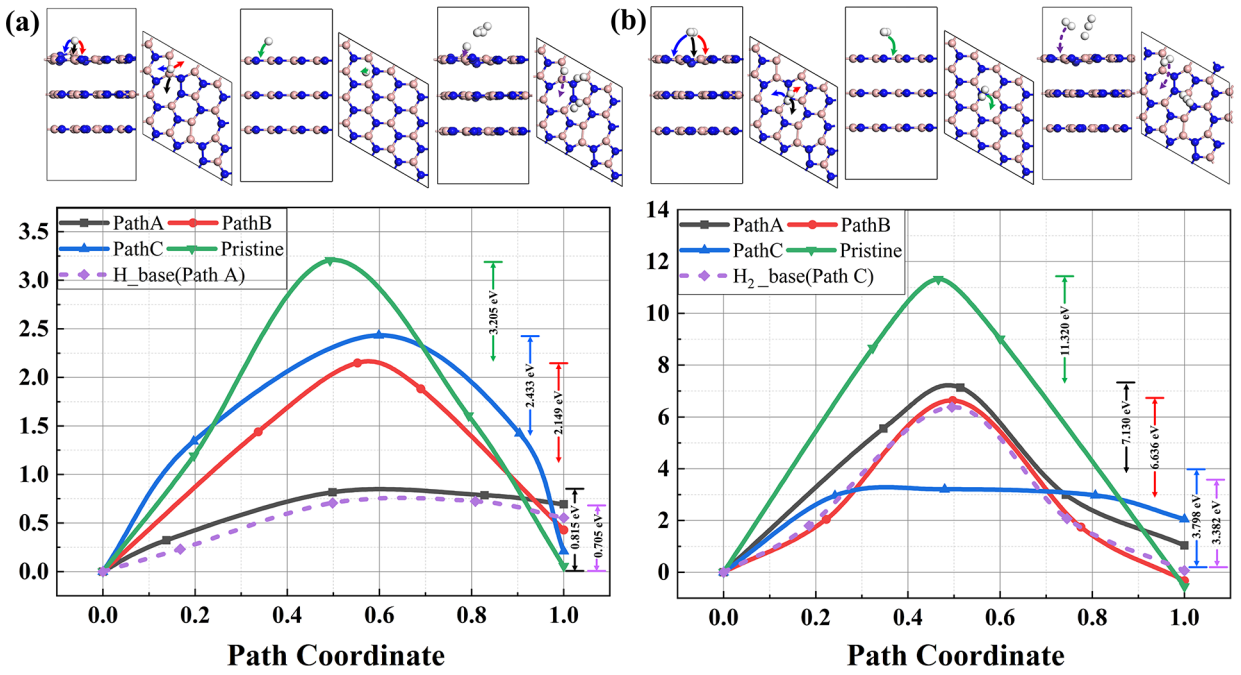

Figure 11. Schematic diagram shows the migration of (a) hydrogen atom and (b) H_2 molecule from their most stable adsorption sites (H-TB1 and H_2-TN2) into the interior of the h-BN(SW) model through adjacent ring bond centers, along with the corresponding energy barrier in single adsorption and coadsorption configurations. For comparison, another schematic diagram illustrates the migration of (a) hydrogen atom and (b) H_2 molecule from their most stable adsorption sites (H-TB1 and H_2-TN2), passing through the hollow site of a regular six-membered-ring bond to reach the interior of the pristine h-BN model, showing its corresponding energy barrier.

single hydrogen atoms at the TB1 site. Notably, it was found that the hydrogen atom closest to the h-BN(SW) surface contributed significantly to orbital hybridization, while other hydrogen atoms showed no contribution to DOS at or above the Fermi level. As anticipated, coadsorption of H_2 molecules at TN1 and TN2 sites did not induce significant changes in state density; thus, the state spectra at CBM and VBM remained composed primarily of B 2p and N 2p states. Our

https://doi.org/10.1021/acsomega.4c02990
ACS Omega 2024, 9, 34597−34607

calculations suggest that interactions between the h-BN(SW) surface and adsorbed atoms mainly occurs between hydrogen atoms closest to the adsorbent surface and boron/nitrogen atoms. Layer-resolved PDOS analysis for coadsorption configuration of H_2-TN2_H-TB1TN1TN3 in Figure 9b reveals an appearance of midgap states within total state density contributed by orbital hybridization involving H 1s and N 2P states, which is inconsistent with single adsorption behavior observed for H_2 molecules at TN_2 site alone. Combined with results from geometric optimization studies, this demonstrates that the remaining single hydrogen atom without stable dimer formation weakly chemisorbs onto the h-BN(SW) surface when increasing number of hydrogen atoms are present at different initial adsorption sites in this H_2-based coadsorption system. Similarly, VCM and VBM still consist primarily of B 2pand N 2p states.

3.3. Migration Behavior of Hydrogen Atom and H_2 Molecule. The migration process of hydrogen atoms and H_2 molecules usually involves at least two possible stages: surface migration and migration from the surface to the subsurface. Based on an analysis of adsorption characteristics, the CI-NEB method was used to further assess the migration behavior of hydrogen atoms and H_2 molecules along different paths on two model surfaces, including an h-BN(SW) model and a pristine h-BN model.

The H-TB1 site was chosen as the final state of migration paths in Figure 10a due to its stability as a single adsorption site for hydrogen atoms. Subsequently, three possible migration paths (A ∼ C) were calculated via typical adsorption sites (H-B3, H-TB2, and H-TB4). These paths exhibited relatively high migration barriers over the h-BN(SW) surface: 1.976, 2.706, and 1.975 eV, respectively. In contrast, the pristine h-BN surface showed good migration properties for hydrogen atoms with barriers ranging from 0.177 to 0.505 eV due to hindrance caused by high adsorption energy on the h-BN(SW) surface. From Figure 10b, the most stable single adsorption site for H_2 molecules (H_2-TN2) was set as the final site of the migration path, while three adjacent adsorption sites (H_2-TB4, H_2-TN4, and H_2-TN3) were selected as initial sites. Among them, path B had the highest barrier of only 0.284 eV compared to other paths with barriers of 0.237 and 0.251 eV, respectively. Similarly, when considering a pristine h-BN model surface, calculated barriers corresponding to these same migration paths ranged from 0.184 to 0.211e V. Overall, we found that compared to the pristine h-BN surface, the h-BN(SW) surface is less conducive to surface migration of hydrogen atoms due to lower adsorption energy providing less resistance against H_2 molecule's migration.

The migration of a hydrogen atom or H_2 molecule from the surface to the interlayer between the first and second layers has been considered as one of the main steps to enter the interior of the h-BN model. As shown in Figure 11a, a barrier of at least 0.815 eV needs to be overcome when a hydrogen atom migrates from the most stable single adsorption site (H-TB1) to the subsurface through an adjacent ring bond center in the h-BN(SW) model, namely path A, whereas in the pristine h-BN model, this figure reaches 3.205 eV. For the same migration path A, the corresponding migration barrier in the most stable H-based coadsorption configuration is 0.705 eV. It can be seen that hydrogen atoms tend to follow path A, migrating inward from the h-BN(SW) surface with SW defects, that is, through the center of adjacent heptagonal boron−nitrogen rings. From Figure 11b, H_2 molecules migrating from their stable single adsorption site (H_2-TN2) through the h-BN(SW) surface layer show an obvious energetic hindrance and even reach 7.130 eV along path A compared to hydrogen atom migration. Similarly, H_2 molecules migrate through regular six-membered rings in pristine h-BN models and reach a highest barrier value of 11.320 eV. For the most stable H_2-based coadsorption case, there is only a slight decrease of 0.416 eV in height for the migration barrier along path C, demonstrating that coadsorption systems have very weak effects on vertical migration of H_2 molecules.

4. CONCLUSIONS

First-principles calculations based on DFT were performed to study the adsorption of residual gas on the surface of h-BN based memristors, with typical SW GBs in the resistance layers. First, the adsorption characteristics, such as adsorption energy, geometric parameters, and charge transfer, were investigated. The results demonstrated that the H-TB1 site and H_2-TN2 site exhibited the most favorable adsorption properties with the lowest adsorption energies (−2.6956 and −0.0899 eV) and shortest bond distances between hydrogen and boron atoms (1.234 and 2.680 Å), respectively. Additionally, charge transfers of 0.5543 and 0.0395*e* were observed for these sites, respectively. The projected band structure and partial density of states (PDOS) analysis revealed that hydrogen atoms tend to chemisorb onto the TB1 site while physically adsorbing onto the TN2 site when forming an H_2 molecule. Furthermore, the two most stable adsorption configurations were obtained for each stable coadsorption configuration: H-TB1_H_2-TN1TN2 and H_2-TN2_H-TB1TN1TN3, where a hydrogen atom and an H_2 molecule are preferentially adsorbed at the TB1 site and TN2 site, respectively. In the H-based case, the dissociation of the H_2 molecule is not evident, and an increase in the number of H_2 molecules does not significantly enhance the adsorption strength of hydrogen atoms. Conversely, in the H_2-based case, adjacent pairs of hydrogen atoms tend to form stable dimer configurations when an even number of hydrogen atoms is present; however, additional individual hydrogen atoms tend to weakly chemisorb onto the h-BN(SW) surface. Finally, the migration barriers of hydrogen atoms and H_2 molecules on the surface of the two h-BN models illustrated that the pristine h-BN surface is more favorable for hydrogen atom migration, while H_2 molecules with lower adsorption energies experience lower migration energy barriers during the migration process. Our calculations also suggest that migrating through the center of adjacent heptagonal boron−nitrogen becomes more difficult for H_2 molecules compared to hydrogen atoms due to a minimum barrier energy difference (3.798 eV for the H_2 molecule vs 0.815 eV for the hydrogen atom). Additionally, the migration barriers for hydrogen atoms and H_2 molecules in the most stable coadsorption configurations of H-based and H_2-based are 0.705 and 3.382 eV, respectively. Thus, our results can actively promote the industrial production of boron nitride-based memristor.

■ ASSOCIATED CONTENT

Data Availability Statement

The data that support the findings of this study are available within the article.

https://doi.org/10.1021/acsomega.4c02990
ACS Omega 2024, 9, 34597−34607

AUTHOR INFORMATION

Corresponding Authors

Jin Yang − *Anhui Province Key Laboratory of Simulation and Design for Electronic Information System (Hefei Normal University), Hefei 230601, PR China*; orcid.org/0009-0005-0155-5846; Email: 1830653979@qq.com

Yuehua Dai − *School of Integrated Circuits, Anhui University, Hefei 230601, PR China*; Email: 15656095630@163.com

Authors

Cheng Ding − *Anhui Province Key Laboratory of Simulation and Design for Electronic Information System (Hefei Normal University), Hefei 230601, PR China*

Yue Chen − *Anhui Province Key Laboratory of Simulation and Design for Electronic Information System (Hefei Normal University), Hefei 230601, PR China*

Shibin Lu − *Anhui Province Key Laboratory of Simulation and Design for Electronic Information System (Hefei Normal University), Hefei 230601, PR China*

Complete contact information is available at: https://pubs.acs.org/10.1021/acsomega.4c02990

Notes

The authors declare no competing financial interest.

ACKNOWLEDGMENTS

This work was supported by National Natural Science Foundation of China (grant no. 61874001), University Natural Science Research Project of Anhui Province (grant no. 2022AH052149, 2023AN051313), Electronic information system simulation design Anhui Province key laboratory open fund project (grant no. 2023ZDSYS03), Hefei Normal University high-level talent research fund project (grant no. 2023rcjj01), and the Enterprise Commissioned Development Project (grant no. HXXM2022100, HXXM2022293 and HXXM2022155).

REFERENCES

(1) Choi, W. B.; Chae, S.; Bae, E.; Lee, J.-W.; Cheong, B.-H.; Kim, J.-R.; Kim, J.-J. Carbon-nanotube-based nonvolatile memory with oxide−nitride−oxide film and nanoscale channel. *Appl. Phys. Lett.* **2003**, *82* (2), 275−277.

(2) Wan, S.; Li, Y.; Li, W.; Mao, X.; Wang, C.; Chen, C.; Dong, J.; Nie, A.; Xiang, J.; Liu, Z.; et al. Nonvolatile ferroelectric memory effect in ultrathin α-In_2Se_3. *Adv. Funct. Mater.* **2019**, *29* (20), 1808606.

(3) Lee, D.; Kim, S.; Kim, Y.; Cho, J. H. One-transistor−one-transistor (1T1T) optoelectronic nonvolatile MoS_2 memory cell with nondestructive read-out. *ACS Appl. Mater. Interfaces* **2017**, *9* (31), 26357−26362.

(4) Shen, Z.; Zhao, C.; Qi, Y.; Xu, W.; Liu, Y.; Mitrovic, I. Z.; Yang, L.; Zhao, C. Advances of RRAM devices: Resistive switching mechanisms, materials and bionic synaptic application. *Nanomaterials* **2020**, *10* (8), 1437.

(5) Shin, H. W.; Son, J. Y. Resistive switching characteristics of graphene/NiO/highly ordered pyrolytic graphite resistive random access memory capacitors. *J. Alloys Compd.* **2019**, *772*, 900−904.

(6) Chen, H.-Y.; Tian, H.; Gao, B.; Yu, S.; Liang, J.; Kang, J.; Zhang, Y.; Ren, T.-L.; Wong, H.-S. P. Electrode/oxide interface engineering by inserting single-layer graphene: Application for HfO_x-based resistive random access memory. In *2012 International Electron Devices Meeting*; IEEE, 2012, pp 20.5.1−20.5.4..

(7) Uchida, Y.; Kawahara, K.; Fukamachi, S.; Ago, H. Chemical vapor deposition growth of uniform multilayer hexagonal boron nitride driven by structural transformation of a metal thin film. *ACS Appl. Electron. Mater.* **2020**, *2* (10), 3270−3278.

(8) Glavin, N. R.; Jespersen, M. L.; Check, M. H.; Hu, J.; Hilton, A. M.; Fisher, T. S.; Voevodin, A. A. Synthesis of few-layer, large area hexagonal-boron nitride by pulsed laser deposition. *Thin Solid Films* **2014**, *572*, 245−250.

(9) Puglisi, F. M.; Larcher, L.; Pan, C.; Xiao, N.; Shi, Y.; Hui, F.; Lanza, M. 2D h-BN based RRAM devices. In *2016 IEEE International Electron Devices Meeting (IEDM)*; IEEE, 2016, pp 34.8.1−34.8.4..

(10) Pan, C.; Ji, Y.; Xiao, N.; Hui, F.; Tang, K.; Guo, Y.; Xiaoming, X.; Puglisi, F. M.; Larcher, L.; Miranda, E.; et al. Coexistence of grain-boundaries-assisted bipolar and threshold resistive switching in multilayer hexagonal boron nitride. *Adv. Funct. Mater.* **2017**, *27* (10), 1604811.

(11) Pan, C.; Miranda, E.; Villena, M. A.; Xiao, N.; Jing, X.; Xie, X.; Wu, T.; Hui, F.; Shi, Y.; Lanza, M. Model for multi-filamentary conduction in graphene/hexagonal-boron-nitride/graphene based resistive switching devices. *2D Mater.* **2017**, *4* (2), 025099.

(12) Ranjan, A.; Raghavan, N.; O'shea, S. J.; Mei, S.; Bosman, M.; Shubhakar, K.; Pey, K. L. Conductive atomic force microscope study of bipolar and threshold resistive switching in 2D hexagonal boron nitride films. *Sci. Rep.* **2018**, *8* (1), 2854.

(13) Dastgeer, G.; Abbas, H.; Kim, D. Y.; Eom, J.; Choi, C. Synaptic Characteristics of an Ultrathin Hexagonal Boron Nitride (h-BN) Diffusive Memristor. *Phys. Status Solidi RRL* **2021**, *15* (1), 2000473.

(14) Hui, F.; Villena, M. A.; Fang, W.; Lu, A.-Y.; Kong, J.; Shi, Y.; Jing, X.; Zhu, K.; Lanza, M. Synthesis of large-area multilayer hexagonal boron nitride sheets on iron substrates and its use in resistive switching devices. *2D Mater.* **2018**, *5* (3), 031011.

(15) Villena, M. A.; Hui, F.; Liang, X.; Shi, Y.; Yuan, B.; Jing, X.; Zhu, K.; Chen, S.; Lanza, M. Variability of metal/h-BN/metal memristors grown via chemical vapor deposition on different materials. *Microelectron. Reliab.* **2019**, *102*, 113410.

(16) Lin, W.; Zhuang, P.; Akinwande, D.; Zhang, X.-A.; Cai, W. Oxygen-assisted synthesis of hBN films for resistive random access memories. *Appl. Phys. Lett.* **2019**, *115* (7), 073101.

(17) Knobloch, T.; Illarionov, Y. Y.; Ducry, F.; Schleich, C.; Wachter, S.; Watanabe, K.; Taniguchi, T.; Mueller, T.; Waltl, M.; Lanza, M.; et al. The performance limits of hexagonal boron nitride as an insulator for scaled CMOS devices based on two-dimensional materials. *Nat. Electron.* **2021**, *4*, 98−108.

(18) Lee, J. S.; Choi, S. H.; Yun, S. J.; Kim, Y. I.; Boandoh, S.; Park, J.-H.; Shin, B. G.; Ko, H.; Lee, S. H.; Kim, Y.-M.; et al. Wafer-scale single-crystal hexagonal boron nitride film via self-collimated grain formation. *Science* **2018**, *362* (6416), 817−821.

(19) Chen, T.-A.; Chuu, C.-P.; Tseng, C.-C.; Wen, C.-K.; Wong, H.-S. P.; Pan, S.; Li, R.; Chao, T.-A.; Chueh, W.-C.; Zhang, Y.; et al. Wafer-scale single-crystal hexagonal boron nitride monolayers on Cu (111). *Nature* **2020**, *579* (7798), 219−223.

(20) Yildirim, H.; Pachter, R. Mechanistic analysis of oxygen vacancy-driven conductive filament formation in resistive random access memory metal/NiO/metal structures. *ACS Appl. Mater. Interfaces* **2018**, *10* (11), 9802−9816.

(21) Hao, R.; Shi, J.; Zhu, L.; Ji, L.; Sun, T.; Feng, S. A first-principle study on adsorption of atomic hydrogen on the two-dimensional hexagonal boron nitride monolayer. *Superlattices Microstruct.* **2017**, *111*, 696−703.

(22) Petrushenko, I. K.; Petrushenko, K. B. Hydrogen adsorption on graphene, hexagonal boron nitride, and graphene-like boron nitride-carbon heterostructures: A comparative theoretical study. *Int. J. Hydrogen Energy* **2018**, *43* (2), 801−808.

(23) Kresse, G.; Joubert, D. From ultrasoft pseudopotentials to the projector augmented-wave method. *Phys. Rev. B* **1999**, *59* (3), 1758−1775.

(24) Delley, B. From molecules to solids with the DMol3 approach. *J. Chem. Phys.* **2000**, *113* (18), 7756−7764.

(25) Li, J. L.; He, T.; Yang, G. Ferromagnetism and semiconducting of boron nanowires. *Nanoscale Res. Lett.* **2012**, *7*, 678.

https://doi.org/10.1021/acsomega.4c02990
ACS Omega 2024, 9, 34597−34607

(26) Perdew, J. P.; Burke, K.; Ernzerhof, M. Generalized gradient approximation made simple. *Phys. Rev. Lett.* **1996**, *77* (18), 3865−3868.
(27) Goerigk, L. A comprehensive overview of the DFT-D3 London-dispersion correction. In *Non-Covalent Interactions in Quantum Chemistry and Physics*; Elsevier, 2017; pp 195−219..
(28) Henkelman, G.; Uberuaga, B. P.; Jónsson, H. A climbing image nudged elastic band method for finding saddle points and minimum energy paths. *J. Chem. Phys.* **2000**, *113* (22), 9901−9904.
(29) Xu, Z.; Lv, X.; Chen, J.; Jiang, L.; Lai, Y.; Li, J. Dispersion-corrected DFT investigation on defect chemistry and potassium migration in potassium-graphite intercalation compounds for potassium ion batteries anode materials. *Carbon* **2016**, *107*, 885−894.
(30) Enujekwu, F. M.; Zhang, Y.; Ezeh, C. I.; Zhao, H.; Xu, M.; Besley, E.; George, M. W.; Besley, N. A.; Do, H.; Wu, T. N-doping enabled defect-engineering of MoS_2 for enhanced and selective adsorption of CO_2: A DFT approach. *Appl. Surf. Sci.* **2021**, *542*, 148556.
(31) Ding, C.; Dai, Y.; Wang, F.; Li, X.; Gao, J.; Yang, B.; Lu, W.; Yang, F. Effect of the coexistence of active metals and boron vacancies on the performance of 2D hexagonal boron nitride resistance memory. *Vacuum* **2022**, *196*, 110747.
(32) Ding, C.; Dai, Y.; Yang, B.; Li, X.; Wang, F.; Yang, F.; Lu, W.; Ke, Q.; Feng, Z. Density functional theory study on Ti/h-BN interface in resistance random access memory device. *J. Phys. D Appl. Phys.* **2022**, *55* (35), 355101.
(33) Ding, C.; Chen, Y.; Yang, J.; Wang, F.; Lu, S.; Li, X.; Dai, Y. First-principles study of graphene intercalation in h-BN based resistance random access memory. *Mater. Today Commun.* **2023**, *36*, 106907.
(34) Priska, Z.; Hidayati, S.; Sholihun, S.; Amalia, W.; Nurwantoro, P. Hydrogen and Water Adsorptions on Monolayer Hexagonal Boron Nitride (h-BN): The First-Principles Calculations. *Key Eng. Mater.* **2021**, *884*, 387−393.

https://doi.org/10.1021/acsomega.4c02990
ACS Omega 2024, 9, 34597−34607